IEEE Access
Multidisciplinary | Rapid Review | Open Access Journal

Received July 19, 2020, accepted August 9, 2020, date of publication August 18, 2020, date of current version August 31, 2020.

Digital Object Identifier 10.1109/ACCESS.2020.3017539

Trajectory Tracking Control for Parafoil Systems Based on the Model-Free Adaptive Control Method

LINGGONG ZHAO, WEILIANG HE, FEIKAI LV, AND WANG XIAOGUANG
School of Astronautics, Beihang University, Beijing 100191, China
Corresponding author: Weiliang He (heweiliang@buaa.edu.cn)

ABSTRACT Parafoil systems are unique steerable decelerator systems. However, due to the strong nonlinearity caused by the flexibility of the canopy and the suspension lines, the existing dynamic models of parafoil systems are not sufficiently accurate enough; and hence, existing model-dependent control methods are not suitable for practical applications. To effectively eliminate the influence of inaccurate models on trajectory tracking, this paper introduces a novel real-time model-independent control method named the model-free adaptive control (MFAC) method. The stability of the MFAC method is theoretically deduced, and the robustness of this approach is analyzed and demonstrated by the Monte Carlo method. To assess the performance of the MFAC method, a six-degree-of-freedom (DOF) dynamic model is built, and then a series of simulations are performed under different conditions. The simulation results demonstrate the effectiveness of the proposed MFAC method in trajectory tracking. Compared with the proportional/integral/derivative (PID) control method and the active disturbance rejection control (ADRC) method, the MFAC method has higher precision and lower energy consumption, especially under complex disturbance conditions.

INDEX TERMS Parafoil system, dynamics, model-free adaptive control, robustness.

I. INTRODUCTION

The parafoil system is a type of flexible air vehicle consisting of a canopy, suspension lines, a payload, and an airborne guidance unit (AGU), as shown in Fig. 1. The canopy provides lift and drag for the vehicle, and the suspension lines connect the canopy to the payload. Actuators, sensors, computers, and complementary components are housed in the AGU, which is strapped in between the parafoil and the payload or atop the payload. The lateral and longitudinal control of the parafoil system is achieved through the deflection of the steering lines attached to the left and right trailing edge (TE) of the canopy [1]. Asymmetric deflection leads to a turning maneuver, and symmetric deflection provides speed control of impact on the ground. These controls allow the parafoil systems to steer in a horizontal direction during descent [2].

Parafoil systems have been applied for decades to improve the accuracy of the point of impact (PI) [3]. Many researchers have studied some aspects of parafoil systems, such as dynamic modeling [4]–[6], flight testing [7], [8] and control.

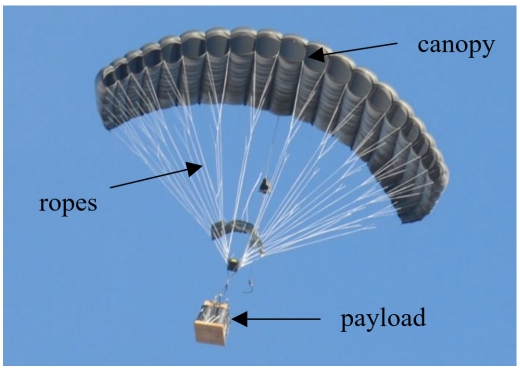

FIGURE 1. Parafoil system.

Nathan Slegers and Mark Costello introduced a model predictive control method for a parafoil system. This method needs a precise mathematical model to project future states and subsequently use these states to determine control actions [9]. Tao and Sun proposed another accurate trajectory tracking control method based on active disturbance rejection control (ADRC). This method could be used without having a precise dynamic model of the parafoil system and

The associate editor coordinating the review of this manuscript and approving it for publication was Chao-Yang Chen.

accounted for external disturbances by utilizing disturbance estimations from an extended state observer (ESO) [10]. Carter *et al.* implemented a proportional/integral/derivative (PID)-based control method for parafoil systems, which had added features to address system constraints and used feed-forward logic to improve response time. The simulations and hardware-in-the-loop flight tests showed that the system achieved an expected delivery accuracy [11].

Most of the abovementioned control methods were not based on parafoil models but simulations or experimental data. The factors contributing to the accuracy of the model are inherent uncertainties in parafoil systems, such as strongly nonlinear systems. For example, the canopy is made of a flexible fabric, which makes it challenging to construct a precise dynamic model. In practical applications, small disturbances could cause changes in the structural shape of the canopy, not to mention the disturbances caused by gusts and control inputs. Structural changes cause changes in aerodynamic forces, which are difficult to simulate through modeling and simulation. Moreover, aerodynamic parameters are not accurate for most parafoil systems, and the computed coefficients should only be used as estimations rather than precise values. Precise aerodynamic parameters are generally obtained from wind tunnel tests, but they are still different from those obtained in real flight tests. Furthermore, the suspension lines attached to the canopy and payload are not always in tension. This phenomenon is difficult to consider in existing dynamic models.

More factors are needed to account for the position and shifting of the pressure center of the flexible canopy, the separation of flow, the forces resulting from flexible TE deflection, the role of derivatives, and a variety of unsteady effects. Hence, a model-independent control method is suitable for parafoil systems.

This paper introduces a new trajectory tracking method for parafoil systems named the model-free adaptive control (MFAC) method, which can be constructed only using input/output (I/O) data. The MFAC method is a data-driven control (DDC) method that was developed by Hou in the 1990s for a discrete-time nonlinear single-input/single-output (SISO) system [12]. The MFAC method relies only on on-line measurement data of a parafoil system and does not depend on any model information or any external test signals. The applicability and effectiveness of this method have been verified through rigorous mathematical analyses and extensive simulations [13]. In 2019, this method was improved and introduced to a category of nonlinear multiple-input/multiple-output (MIMO) systems.

As a representative DDC algorithm, the MFAC algorithm has become a popular research topic in recent years and has been applied in several industrial control fields [14]–[16], such as transportation, oil refining, and chemical processing [19]. In addition, it has been used in vehicle control, such as launch vehicle control and unmanned surface heading control [17] - [19]. The MFAC method controls the attitudes of launch vehicles, and simulations have demonstrated the effectiveness of this control method by comparing it with the traditional PID control method [17]. In reference [18], the improved MFAC method based on iterative feedback tuning (IFT-MFAC) was applied to control three channels of a launch vehicle. In contrast with the PID method, the MFAC method was not sensitive to system time delay or model destabilization in the heading control of an unmanned surface vehicle [19].

This paper applies the MFAC method to parafoil systems, utilizing nothing but real-time I/O data. Hence, this work represents a new solution for parafoil system control and a novel application of the MFAC method. A controller is established for the MFAC method, and its stability and robustness are verified. In addition, using the Monte Carlo method, the robustness of this controller is analyzed through thousands of simulations that imitate real flight situations. To provide corresponding flight data and assess the control performance of the MFAC method, a six-degree-of-freedom (DOF) dynamic model is built, and a series of simulation tests are performed. The results from this method are then compared with those from the PID control method and ADRC method.

II. PARAFOIL SYSTEM DYNAMICS

No dynamic models are required to establish the MFAC algorithm. However, as an on-line control approach, the MFAC method needs real-time system status data to iteratively calculate the value of the control input in simulations. In addition, the control performance of the MFAC controller should be evaluated by a simulated dynamic model. Therefore, a six-DOF dynamic model of the parafoil system is established in this section. This model transmits the system status data to the controller module and receives the value of the control input.

With the exception of movable parafoil brakes, the parafoil canopy is considered to be a fixed shape once it has completely inflated with the suspension lines in tension. The whole system is considered a rigid body in the simulations, which is the fundamental hypothesis adopted by most researchers. The dynamic system used in this work has six DOFs. As shown in Fig. 2, three coordinate systems are used: the body-fixed frame $\{b\}$, the wind frame $\{w\}$, and the initial frame $\{i\}$ [20].

The body-fixed frame is fixed to the center of mass of the system and comprises the following axes:

- x_b: positive direction is forward along the longitudinal axis of the system in the plane of symmetry of the system;
- z_b: positive direction points down in the plane of symmetry of the system, perpendicular to the x_b axis;
- y_b: perpendicular to the x_b -z_b plane, wherein the positive direction is determined by the right-hand rule.

The wind frame $\{w\}$ is originally at the center of gravity of the system and comprises the following axes:

- x_w: positive direction is forward along the direction of the velocity vector relative to the air;

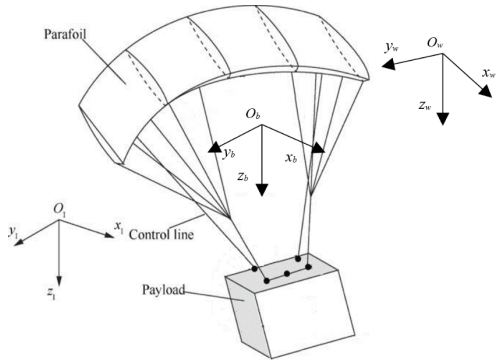

FIGURE 2. Dynamic model of the parafoil system.

- z_w: positive direction points down in the plane of symmetry of the system, perpendicular to the x_w axis;
- y_w: perpendicular to the x_w-z_w plane, wherein the positive direction is determined by the right-hand rule.

The initial frame $\{i\}$ is fixed relative to the surface of the Earth and comprises the following axes:

- x_i: positive direction is true North;
- y_i: positive direction is to the East;
- z_i: positive direction is towards the center of the Earth.

According to Newton's second law and rotational dynamics, dynamic equations are formed by summing the forces and moments about the center of mass of the system and equating them to the time derivations of the linear and angular velocity. The dynamic functions of the parafoil system are expressed as follows:

$$\begin{aligned}(m+m_{app})\begin{bmatrix}\dot{u}\\ \dot{v}\\ \dot{w}\end{bmatrix} &= F_b - mS(\omega)\begin{bmatrix}u\\ v\\ w\end{bmatrix} + F_{app}\\ &= {}^b_gR\cdot G + {}^b_aR\cdot F_a - mS(\omega)\begin{bmatrix}u\\ v\\ w\end{bmatrix} + F_{app} \quad (1)\end{aligned}$$

$$(I+I_{app})\begin{bmatrix}\dot{p}\\ \dot{q}\\ \dot{r}\end{bmatrix} = M_b - S(\omega)I\begin{bmatrix}p\\ q\\ r\end{bmatrix} + M_{app} \quad (2)$$

where $[u\ v\ w]^T$ is the velocity of the system in trame $\{b\}$; $[p\ q\ r]^T$ is the angular velocity of the system in frame $\{b\}$; m and I are the mass and inertial mass of the system, respectively; F, G and M represent the force, gravity, and moment, respectively, for which the subscript indicates the frame; m_{app} represents the apparent mass; and F_{app} and M_{app} represent the mean force and moment about the apparent mass. The apparent mass of the system is ignored to simplify the model simulation.

${}^b_iR$ is the transformation matrix from the initial frame to the body frame, which is expressed as follows:

$${}^b_iR = \begin{bmatrix} c_\psi c_\theta & s_\psi c_\theta & -s_\theta \\ c_\psi s_\theta s_\phi - s_\psi c_\phi & s_\psi s_\theta s_\phi + c_\psi c_\phi & c_\theta s_\phi \\ c_\psi s_\theta c_\phi + s_\psi s_\phi & s_\psi s_\theta c_\phi - c_\psi s_\phi & c_\theta c_\phi \end{bmatrix} \quad (3)$$

where φ, θ, and ψ are the roll, pitch and yaw, respectively, and **c** and **s** are sine and cosine functions, respectively, as shown in the following expression:

$$c \equiv \cos, \quad s \equiv \sin.$$

${}^b_wR$ is the transformation matrix from the wind frame $\{w\}$ to the body frame $\{b\}$, which is expressed as follows:

$${}^b_wR = \begin{bmatrix} c_\alpha c_\beta & c_\alpha s_\beta & -s_\alpha \\ -s_\beta & c_\beta & 0 \\ s_\alpha c_\beta & s_\alpha s_\beta & c_\alpha \end{bmatrix} \quad (4)$$

The angle of attack α and angle of sideslip β are determined by the components of the airspeed vector V_a in the $\{b\}$ coordination system, $[v_x, v_y, v_z]$, as shown in the following equation:

$$\alpha = \tan^{-1}\left(\frac{v_z}{v_x}\right), \quad \beta = \tan^{-1}\left(\frac{v_y}{\sqrt{v_x^2+v_z^2}}\right). \quad (5)$$

The dynamics equations are established in body-fixed frame which is non-inertial frame, therefore, a skew-symmetric matrix, $S(\omega)$, is used which is expressed as follows:

$$S(\omega) = \begin{bmatrix} 0 & -r & q \\ r & 0 & -p \\ -q & p & 0 \end{bmatrix}. \quad (6)$$

F_a is the aerodynamic force in the $\{w\}$ frame, which can be expressed as follows:

$$F_a = \frac{1}{2}\rho V_a^2 S \begin{bmatrix} C_{D0} + C_{D\alpha^2}\alpha^2 + C_{D\delta_s}\delta_s \\ C_{Y\beta}\beta \\ C_{L0} + C_{L\alpha}\alpha + C_{L\delta_s}\delta_s \end{bmatrix}, \quad (7)$$

$$M_b = \frac{\rho V_a^2 S}{2}\begin{bmatrix} b\left(C_{l\beta}\beta + \frac{b}{2V_a}C_{lp}p + \frac{b}{2V_a}C_{lr}r + C_{l\delta_a}\delta_a\right) \\ c\left(C_{m0} + C_{m\alpha}\alpha + \frac{c}{2V_a}C_{mq}q\right) \\ b\left(C_{n\beta}\beta + \frac{b}{2V_a}C_{np}p + \frac{b}{2V_a}C_{nr}r + C_{n\delta_a}\delta_a\right) \end{bmatrix} \quad (8)$$

where C_{D0}, $C_{D\alpha 2}$, $C_{D\delta s}$, $C_{Y\beta}$, C_{L0}, $C_{L\alpha}$, $C_{L\delta s}$ $C_{l\beta}$, C_{lp}, C_{lr}, $C_{l\delta a}$, C_{m0}, $C_{m\alpha}$, C_{mq}, $C_{n\beta}$, C_{np}, C_{nr}, and $C_{n\delta a}$ are aerodynamic coefficients, S is the area of the canopy, ρ is the density of the environment, δ_s is symmetric TE deflection, δ_a is asymmetric TE deflection, and δ_l and δ_r represent the left-side and right-side TE deflection, respectively. Accordingly, the symmetric and asymmetric TE deflection can be expressed as follows:

$$\delta_a = \delta_l - \delta_r, \quad \delta_s = \min(\delta_l, \delta_r) \quad (9)$$

The kinematic equations of the parafoil system are as follows and each part has been mentioned above. The wind velocity is expressed in inertial frame.

$$\begin{bmatrix} v_x \\ v_y \\ v_z \end{bmatrix} = \begin{bmatrix} u \\ v \\ w \end{bmatrix} - {}^b_iR\begin{bmatrix} wind_x \\ wind_y \\ wind_z \end{bmatrix} \quad (10)$$

$$\begin{bmatrix} \dot{\phi} \\ \dot{\theta} \\ \dot{\psi} \end{bmatrix} = \begin{bmatrix} 1 & s_\phi s_\theta / c_\theta & c_\phi s_\theta / c_\theta \\ 0 & c_\phi & -s_\phi \\ 0 & s_\phi / c_\theta & c_\phi / c_\theta \end{bmatrix} \begin{bmatrix} p \\ q \\ r \end{bmatrix} \tag{11}$$

III. CONTROLLER CONSTRUCTION

The model-free control method—a typical DDC method—was first proposed by Hou in 1994 for a class of discrete-time nonlinear systems. In this method, only the measured I/O data from the controlled closed-loop system are used for controller design and stability analysis, without any model dynamics. The stability and convergence of the MFAC scheme for a regulation problem were proposed in 2011 by Pro. Hou [21].

The essential idea of the MFAC method is to use an equivalent linearized dynamic model and a novel pseudopartial derivative (PPD) at the current operation point to represent the general discrete-time nonlinear system [21]. The MFAC controller design process is detailed hereafter.

For a nonlinear discrete-time system, the following expression can be obtained:

$$y_{k+1} = f(y_k, y_{k-1}, \cdots, y_{k-n_y}, u_k, u_{k-1}, \cdots, u_{k-n_u}) \tag{12}$$

where $u_k \in R^m$ and $y_k \in R^m$ are the system input and output at time k, respectively, and n_y and n_u are integers.

The nonlinear system (12) satisfies the Lipschitz condition, except for finite moments [22]. Hence,for $\forall\ k_1 \neq k_2$, k_1, $k_2 \geq 0$ and $u_{k1} \neq u_{k2}$, the system obeys the following inequality:

$$\left\| y_{k_1+1} - y_{k_2+1} \right\| \leq b \left\| u_{k_1} - u_{k_2} \right\| \tag{13}$$

where b is a constant and $b > 0$.

There exists a time-varying parameter Ω_k, named the PPD, and the system can be described with the following expression:

$$y_{k+1} = y_k + \Omega_k \Delta u_k, \tag{14}$$

$$\Delta y_{k+1} = \Omega_k \Delta u_k \tag{15}$$

The estimation algorithm for the time-varying parameter should be considered to design an optimal controller. The criterion function of the control input is established as shown in (16).

$$R(u_k) = \left\| y^d_{k+1} - y_{k+1} \right\|^2 + \alpha \left\| u_k - u_{k-1} \right\|^2 \tag{16}$$

where $\alpha > 0$ is the weighting factor for penalizing drastic input changes and y^d_{k+1} is the desired output.

By taking a derivative with respect to u_k and substituting (14) into the function, the following expression can be obtained:

$$\frac{\partial R(u_k)}{\partial u_k} = -2\Omega_k \left[y^d_{k+1} - y_k - \Omega_k (u_k - u_{k-1}) \right] u_k + 2\alpha (u_k - u_{k-1}) \tag{17}$$

Then, by setting the function equal to zero and simplifying, the following expression is obtained:

$$u_k = u_{k-1} + \frac{\Omega_k}{\alpha + (\Omega_k)^2} (y^d_{k+1} - y_k) \tag{18}$$

Similar to the estimated input function, the PPD criterion function should be constructed as follows:

$$R(\Omega_k) = |\Delta y_k - \Omega_k \Delta u_{k-1}|^2 + \tau \left| \Omega_k - \Omega_{k-1} \right|^2 \tag{19}$$

where $\tau > 0$ is the weighting factor for penalizing drastic changes in the PPD values.

By taking a derivative with respect to Ω_k, setting the function equal to zero and simplifying, the following expression is obtained:

$$\frac{\partial R(\Omega_k)}{\Omega_k} = -2(\Delta y_k - \Omega_k \Delta u_{k-1}) \Delta u_{k-1} + 2\tau (\Omega_k - \Omega_{k-1}) = 0 \tag{20}$$

Then, the PPD estimation function is expressed as follows:

$$\begin{aligned} \hat{\Omega}_k &= \frac{\tau}{\tau + \Delta u^2_{k-1}} \hat{\Omega}_{k-1} + \frac{\Delta y \Delta u_{k-1}}{\tau + \Delta u^2_{k-1}} \\ &= \hat{\Omega}_{k-1} + \frac{\Delta u_{k-1}}{\tau + \Delta u^2_{k-1}} (\Delta y_k - \hat{\Omega}_{k-1} \Delta u_{k-1}) \end{aligned} \tag{21}$$

where $\hat{\Omega}$ is an estimation of the system PPD Ω.

Hence, the control strategy has been proposed and expressed as follows:

$$\hat{\Omega}_k = \hat{\Omega}_{k-1} + \frac{\kappa \Delta u_{k-1}}{\tau + \Delta u^2_{k-1}} (\Delta y_k - \hat{\Omega}_{k-1} \Delta u_{k-1}) \tag{22}$$

$$u_k = u_{k-1} + \frac{\beta \hat{\Omega}_k (y^d_{k+1} - y_k)}{\alpha + \left(\hat{\Omega}_k \right)^2} \tag{23}$$

where $\beta \in (0,1]$ and $\kappa \in (0,1]$ are stepping factors and $\tau > 0$ and $\alpha > 0$ are weighting factors.

β and κ are substituted into the control functions to make them more universal and control the convergence speed of the estimated PPD or control value.

A resetting algorithm is proposed to strengthen the controlling effect of the time-varying system.

If $\left| \hat{\Omega}_k \right| \leq \varepsilon, \quad |\Delta u_{k-1}| \leq \varepsilon$ or $sign(\hat{\Omega}_k) \neq sign(\hat{\Omega}_1)$,

then $\hat{\Omega}_k = \hat{\Omega}_1$, where ε is a small positive real number.

The final MFAC functions of the discrete-time nonlinear system are given as shown in (18) and (20). A process flow diagram of the MFAC method is presented in Fig. 3.

IV. STABILITY AND ROBUSTNESS ANALYSIS

Having proposed the MFAC controller functions, the stability and robustness of this method must be analyzed. Two steps are performed to analyze the stability of the MFAC method: the first step is to analyze the stability of the estimated PPD, whereas the second step is to analyze the stability of the MFAC method. The approach to the robustness analysis is similar to that used for the stability analysis.

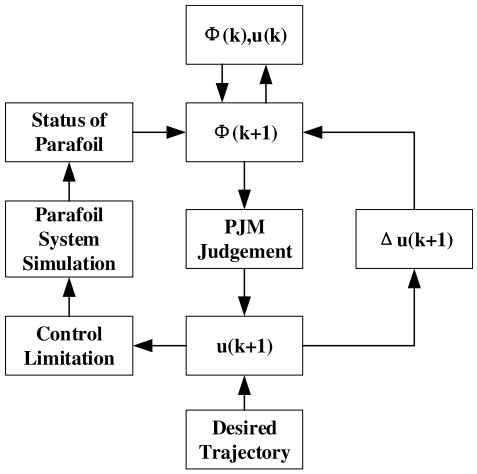

FIGURE 3. Process flow diagram of the MFAC method.

A. STABILITY ANALYSIS OF THE ESTIMATED PPD

In this section, the stability of the estimated PPD is analyzed briefly.

First, a nonlinear system should be described in mathematical form. For a nonlinear system that satisfies (13)-(15), $|\Omega_k| \leq b$ is reasonable.

If $\hat{\Omega}_k$ satisfies the following conditions, it has obvious bounds:

$$\left|\hat{\Omega}_k\right| \leq \varepsilon, \quad |\Delta u_{k-1}| \leq \varepsilon \text{ or } sign(\hat{\Omega}_k) \neq sign(\hat{\Omega}_1)$$

In other conditions, the error in the estimated PPD is defined as follows:

$$\bar{\Omega}_k = \hat{\Omega}_k - \Omega_k \tag{24}$$

By combining (22) and (24), the following equation is obtained:

$$\bar{\Omega}_k = \hat{\Omega}_{k-1} + \frac{\kappa \Delta u_{k-1}}{\tau + \Delta u_{k-1}^2}(\Delta y_k - \hat{\Omega}_{k-1}\Delta u_{k-1}) - \Omega_k \tag{25}$$

This function can be rearranged as follows:

$$\begin{aligned}\bar{\Omega}_k &= (1 - \frac{\kappa \Delta u_{k-1}^2}{\tau + \Delta u_{k-1}^2})\hat{\Omega}_{k-1} + \frac{\kappa \Delta u_{k-1}}{\tau + \Delta u_{k-1}^2}\Delta y_k - \Omega_k \\ &= (1 - \frac{\kappa \Delta u_{k-1}^2}{\tau + \Delta u_{k-1}^2})(\bar{\Omega}_{k-1} + \Omega_{k-1}) \\ &\quad + \frac{\kappa \Delta u_{k-1}}{\tau + \Delta u_{k-1}^2}\Delta y_k - \Omega_k \end{aligned} \tag{26}$$

After additional rearrangement, the following expression can be obtained:

$$\begin{aligned}\bar{\Omega}_k = (1 - \frac{\kappa \Delta u_{k-1}^2}{\tau + \Delta u_{k-1}^2})\bar{\Omega}_{k-1} + \Omega_{k-1} - \Omega_k \\ + \frac{\kappa \Delta u_{k-1}}{\tau + \Delta u_{k-1}^2}(\Delta y_k - \Omega_{k-1}\Delta u_{k-1})\end{aligned} \tag{27}$$

The last part of the function satisfies the nonlinear system definition and is equal to zero. Thus, the function takes the following form:

$$\bar{\Omega}_k = (1 - \frac{\kappa \Delta u_{k-1}^2}{\tau + \Delta u_{k-1}^2})\bar{\Omega}_{k-1} + \Omega_{k-1} - \Omega_k. \tag{28}$$

Then, take the absolute value of this function as follows:

$$\begin{aligned}\left|\bar{\Omega}_k\right| &= \left|(1 - \frac{\kappa \Delta u_{k-1}^2}{\tau + \Delta u_{k-1}^2})\bar{\Omega}_{k-1} + \Omega_{k-1} - \Omega_k\right| \\ &\leq \left|(1 - \frac{\kappa \Delta u_{k-1}^2}{\tau + \Delta u_{k-1}^2})\right|\left|\bar{\Omega}_{k-1}\right| + |\Omega_{k-1} - \Omega_k|\end{aligned} \tag{29}$$

The triangle inequality is used in this equation and is expressed as follows:

$$|a + b| \leq |a| + |b|.$$

Part of the function, $\kappa \Delta u_{k-1}^2/(\tau + \Delta u_{k-1}^2)$, is a monotonically increasing function about Δu_{k-1}^2, and the minimum value of Δu_{k-1} is ε. Thus, this part of the function is not less than $\kappa\varepsilon^2/(\tau + \varepsilon^2)$. Moreover, the coefficient of $\left|\bar{\Omega}_{k-1}\right|$ has the following bounds:

$$0 \leq \left|1 - \frac{\kappa \Delta u_{k-1}^2}{\tau + \Delta u_{k-1}^2}\right| \leq \left|1 - \frac{\kappa \varepsilon^2}{\tau + \varepsilon^2}\right| = D_1 < 1 \tag{30}$$

After simplification, (30) reduces to the following expression:

$$\left|\bar{\Omega}_k\right| \leq D_1\left|\bar{\Omega}_{k-1}\right| + |\Omega_{k-1} - \Omega_k| \tag{31}$$

As previously mentioned, $|\Omega_k| \leq b$. Hence, the second part of (29) can be expressed as follows:

$$|\Omega_{k-1} - \Omega_k| \leq 2b \tag{32}$$

Furthermore, the bounds of the error in the estimated PPD can be expressed as follows:

$$\begin{aligned}\left|\bar{\Omega}_k\right| &\leq D_1\left|\bar{\Omega}_{k-1}\right| + 2b \leq D_1^2\left|\bar{\Omega}_{k-2}\right| + 2bD_1 + 2b \\ &\leq \cdots \leq D_1^{k-1}\left|\bar{\Omega}_1\right| + \frac{2b(1 - D_1^{k-1})_1}{1 - D_1}\end{aligned} \tag{33}$$

Through this deduction, $\left|\bar{\Omega}_k\right|$ is shown to have the same bounds as $\left|\hat{\Omega}_k\right|$, the estimated PPD.

B. STABILITY ANALYSIS OF THE CONTROL SYSTEM

The tracking error of the nonlinear system is defined as follows:

$$E_{k+1} = y^d - y_{k+1} \tag{34}$$

where y^d is the desired trajectory, which remains constant. By substituting (14) into (34), the following expression can be obtained:

$$E_{k+1} = y^d - y_k - \Omega_k \Delta u_k \tag{35}$$

According to (24), Δu_k can be expressed as follows:

$$\Delta u_k = \frac{\beta\hat{\Omega}_k(y^d - y_k)}{\alpha + \left(\hat{\Omega}_k\right)^2} = \frac{\beta\hat{\Omega}_k E_k}{\alpha + \left(\hat{\Omega}_k\right)^2} \tag{36}$$

Hence, the tracking error can be transformed into the following expression:

$$E_{k+1} = (1 - \frac{\beta\hat{\Omega}_k\Omega_k}{\alpha + \left(\hat{\Omega}_k\right)^2})E_k \tag{37}$$

Considering the resetting algorithm, $\hat{\Omega}_k$ and Ω_k remain positive or negative, and $\hat{\Omega}_k\Omega_k$ is positive. Thus, the following expression is correct:

$$0 < M_1 \leq \frac{\hat{\Omega}_k\Omega_k}{\alpha + (\hat{\Omega}_k)^2} \leq \frac{b\hat{\Omega}_{kk}}{\alpha + (\hat{\Omega}_k)^2} \tag{38}$$

The fundamental inequality, shown hereafter, helps to simplify this function:

$$a^2 + b^2 \geq 2ab$$

where a and b are real numbers.

Thus, (38) can be transformed into the following expression:

$$0 < M_1 \leq \frac{b\hat{\Omega}_k}{\alpha + (\hat{\Omega}_k)^2} \leq \frac{b\hat{\Omega}_k}{2\sqrt{\alpha}\hat{\Omega}_k} = \frac{b}{2\sqrt{\alpha}} \tag{39}$$

Since $\alpha > \alpha_{\min} = b^2/4$, the bounds in (39) can be expressed as $0 < M_1 < 1$. Thus, the first part of the tracking error can be expressed as follows:

$$1 - \frac{\beta\hat{\Omega}_k\Omega_k}{\alpha + \left(\hat{\Omega}_k\right)^2} \leq 1 - \beta M_1 = D_2 < 1 \tag{40}$$

Now, reconsider the tracking error and take its absolute value as follows:

$$\begin{aligned} |E_{k+1}| &= \left|(1 - \frac{\beta\hat{\Omega}_k\Omega_k}{\alpha + \left(\hat{\Omega}_k\right)^2})E_k\right| = \left|1 - \frac{\beta\hat{\Omega}_k\Omega_k}{\alpha + \left(\hat{\Omega}_k\right)^2}\right| |E_k| \\ &\leq D_2 |E_k| \end{aligned} \tag{41}$$

Through the iteration algorithm, the astringency of E_k will be verified:

$$|E_{k+1}| \leq D_2 |E_k| \leq \cdots \leq D_2^k |E_1| \tag{42}$$

$$\lim_{k\to\infty} |E_{k+1}| = 0 \tag{43}$$

The increment of the control value is expressed as shown in (36). By taking the absolute value and combining it with (42), the following useful expression can be obtained:

$$\begin{aligned} |\Delta u_k| &= \left|\frac{\beta\hat{\Omega}_k}{\alpha + \left(\hat{\Omega}_k\right)^2}\right| |E_k| \leq \left|\frac{\beta\hat{\Omega}_k}{2\sqrt{\alpha}\hat{\Omega}_k}\right| |E_k| \\ &< \left|\frac{\beta}{b}\right| |E_k| = M_2 |E_k| \end{aligned} \tag{44}$$

$$\lim_{k\to\infty} |\Delta u_k| = 0 \tag{45}$$

where M_2 is a limited number.

Considering the control value function and the iteration method, the control system stability analysis is expressed as follows, which verifies that the control value is bounded.

$$\begin{aligned} |u_k| &= |u_k - u_{k-1} + u_{k-1}| \leq |u_k - u_{k-1}| + |u_{k-1}| \\ &\leq \cdots \leq |u_k - u_{k-1}| + |u_{k-1} - u_{k-2}| \\ &\quad + \cdots + |u_2 - u_1| + |u_1| \\ &= |\Delta u_k| + |\Delta u_{k-1}| + \cdots + |\Delta u_2| + |u_1| \\ &< M_2(|E_k| + |E_{k-1}| + \cdots + |E_2|) + |u_1| \\ &\leq M_2 \frac{d_2}{1 - d_2} |E_1| + |u_1| \end{aligned} \tag{46}$$

As shown in the process above, the estimated PPD and the control value of the MFAC method are both bounded and stable.

C. ROBUSTNESS ANALYSIS

In real flight circumstances, system status data are mixed with disturbances. Hence, y_k^m is remarked as measured status data, which contains the real status and measurement error as follows:

$$y_k^m = y_k + \varsigma_k \tag{47}$$

where ς_k is the measurement error, which has the following bounds:

$$|\varsigma_k| \leq b_m \tag{48}$$

The function of the MFAC method takes the following form, whereas the resetting algorithm remains the same.

$$\hat{\Omega}_k = \hat{\Omega}_{k-1} + \frac{\kappa\Delta u_{k-1}}{\tau + \Delta u_{k-1}^2}(\Delta y_k^m - \hat{\Omega}_{k-1}\Delta u_{k-1}) \tag{49}$$

$$u_k = u_{k-1} + \frac{\beta\hat{\Omega}_k(y_{k+1}^d - y_k^m)}{\alpha + \left(\hat{\Omega}_k\right)^2} \tag{50}$$

Moreover, (25) transforms as follows:

$$\bar{\Omega}_k = \hat{\Omega}_{k-1} + \frac{\kappa\Delta u_{k-1}}{\tau + \Delta u_{k-1}^2}(\Delta y_k^m - \hat{\Omega}_{k-1}\Delta u_{k-1}) - \Omega_k \tag{51}$$

According to the definition of y_k^m, the following expression can be obtained:

$$\Delta y_k^m = \Delta y_k + \Delta\varsigma_k \tag{52}$$

By combining (51) and (52), the following expression can be obtained:

$$\begin{aligned} \bar{\Omega}_k = (1 - \frac{\kappa\Delta u_{k-1}^2}{\tau + \Delta u_{k-1}^2})\bar{\Omega}_{k-1} \\ + \frac{\kappa\Delta u_{k-1}}{\tau + \Delta u_{k-1}^2}\Delta\varsigma_k + \Omega_{k-1} - \Omega_k \end{aligned} \tag{53}$$

If $|\Delta u_{k-1}| \neq 0$, then the following expression is correct:

$$\frac{\kappa\,|\Delta u_{k-1}|}{\tau+\Delta u_{k-1}^2}=\frac{\kappa}{\frac{\tau}{|\Delta u_{k-1}|}+|\Delta u_{k-1}|}\leq\frac{\kappa}{2\sqrt{\tau}} \tag{54}$$

Then, after taking the absolute value of the second part of (53), the following expression can be obtained:

$$\begin{aligned}&\left|\frac{\kappa\Delta u_{k-1}}{\tau+\Delta u_{k-1}^2}\Delta\varsigma_k+\Omega_{k-1}-\Omega_k\right|\\&\leq\left|\frac{\kappa\Delta u_{k-1}}{\tau+\Delta u_{k-1}^2}\right||\Delta\varsigma_k|+|\Omega_{k-1}-\Omega_k|\\&\leq\frac{\kappa b_m}{\tau}+2b\end{aligned} \tag{55}$$

Note that λ and μ are defined as follows, wherein (58) is derived from (53).

$$\lambda=\frac{\kappa b_m}{\tau}+2b \tag{56}$$

$$\mu=1-\frac{\kappa\varepsilon^2}{\tau+\varepsilon^2} \tag{57}$$

$$\begin{aligned}\left|\bar{\Omega}_k\right|&\leq\mu\left|\bar{\Omega}_{k-1}\right|+\lambda\leq\mu^2\left|\bar{\Omega}_{k-2}\right|+\lambda\mu+\lambda\\&\leq\cdots\leq\mu^{k-1}\left|\bar{\Omega}_1\right|+\frac{\lambda}{1-\mu}\end{aligned} \tag{58}$$

Thus, the PPD is still bounded even with the disturbance. The control value should be verified to have bounds.

Note that the definition in (36) transforms as follows:

$$E_{k+1}^m=y^d-y_{k+1}^m=E_{k+1}-\varsigma_{k+1} \tag{59}$$

Moreover, the control value calculating function can be expressed as follows:

$$u_k=u_{k-1}+\frac{\beta\hat{\Omega}_k E_k^m}{\alpha+\left(\hat{\Omega}_k\right)^2}=u_{k-1}+\frac{\beta\hat{\Omega}_k(E_k-\varsigma_k)}{\alpha+\left(\hat{\Omega}_k\right)^2} \tag{60}$$

The PPD and estimated PPD have the following bounds:

$$\hat{\varepsilon}\leq|\Omega_k|\leq b_1 \text{ and } \varepsilon\leq\left|\hat{\Omega}_k\right|\leq b.$$

Hence, the following expression can be deduced:

$$0<D_3=\frac{\beta\varepsilon\hat{\varepsilon}}{\alpha+b^2}\leq\frac{\beta\hat{\Omega}_k\Omega_k}{\alpha+\left(\hat{\Omega}_k\right)^2}\leq\frac{\beta b_1}{2\sqrt{\alpha}}=D_4<1 \tag{61}$$

Furthermore, (59) can be transformed as follows:

$$E_{k+1}^m=y^d-y_{k+1}^m=y^d-y_k^m-\Omega_k\Delta u_k=E_k^m-\Omega_k\Delta u_k \tag{62}$$

By combining (62) with (60), the following expression is obtained:

$$\begin{aligned}\left|E_{k+1}^m\right|&=\left|(1-\frac{\beta\hat{\Omega}_k\Omega_k}{\alpha+\left(\hat{\Omega}_k\right)^2})E_k^m+\frac{\beta\hat{\Omega}_k\Omega_k}{\alpha+\left(\hat{\Omega}_k\right)^2}\varsigma_k\right|\\&\leq\left|1-\frac{\beta\hat{\Omega}_k\Omega_k}{\alpha+\left(\hat{\Omega}_k\right)^2}\right|\left|E_k^m\right|+\left|\frac{\beta\hat{\Omega}_k\Omega_k}{\alpha+\left(\hat{\Omega}_k\right)^2}\right||\varsigma_k|\\&\leq(1-D_3)\left|E_k^m\right|+D_4b_m\\&\leq\cdots\leq(1-D_3)^k\left|E_1^m\right|+\frac{D_4b_m}{D_3}\end{aligned} \tag{63}$$

$$\lim_{k\to\infty}\left|E_{k+1}^m\right|=0 \tag{64}$$

Therefore, E_k^m has bounds. Similar to (44), the control value of the MFAC method has bounds.

According to this discussion, the MFAC method is robust to disturbances.

D. SIMULATIONS OF ROBUSTNESS

The robustness of the MFAC method has been analyzed in theory and is verified by the Monte Carlo method in this section. The disturbances, which fit a normal distribution, are listed in Table 1 [24]. Six parameters are used in the error calculation. Note that all of the standard deviations have been magnified by several times than their actual values and those in the reference. One thousand simulations are carried out.

TABLE 1. Disturbances in the status of the parafoil system.

Parameter	Mean	Standard deviation	Units
V_x	0	1	m/s
V_y	0	1	m/s
V_z	0	1	m/s
φ	0	10	degrees
θ	0	10	degrees
ψ	0	10	degrees

The control performance from the simulations is shown in Fig. 4, which illustrates that the MFAC controller works well in all situations. The maximum distance errors (MDEs) are shown in Fig. 5, wherein the results are taken from every 10 simulations. As shown in this figure, the average value of the MDE in the 1000 simulations is 10.08 m, wherein 90% of

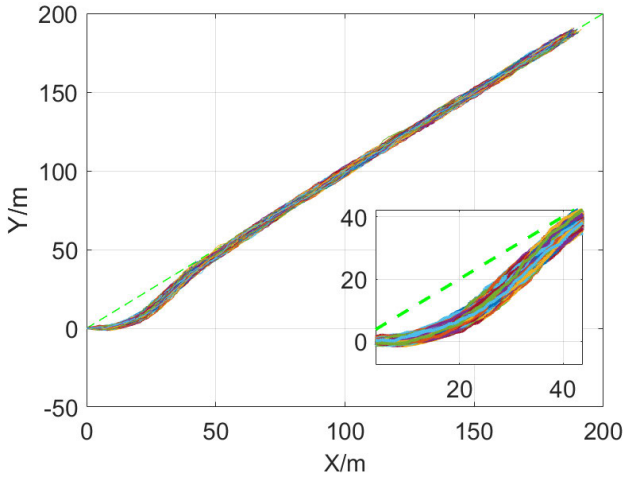

FIGURE 4. Control performance in 1000 simulations.

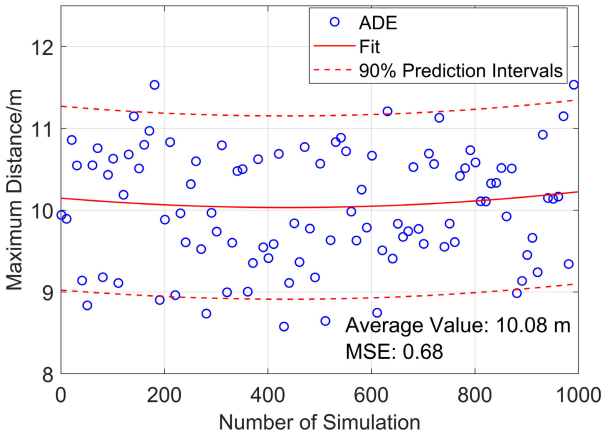

FIGURE 5. Distribution of the MDE in 1000 simulations.

the MDE ranges from 9 m to 11.2 m and the mean square error (MSE) is 0.68. The average distance errors (ADEs) are shown in Fig. 6. The average value of the ADE in the 1000 simulations is 2.26 m, wherein 90% of the ADE ranges from 2 m to 2.5 m and the MSE is 0.127.

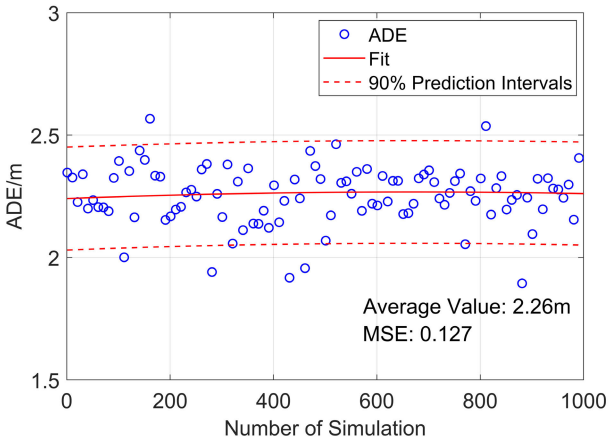

FIGURE 6. Distribution of the ADE in 1000 simulations.

The average control input values in 1000 simulations are also analyzed, and the results are shown in Fig. 7. The average value in this figure is 23.6%, wherein 90% of the results range from 22% to 25% and the MSE is less than 0.01.

These simulations verified that the MFAC method has strong robustness and stability.

V. SIMULATION

A simulation scheme is designed in this section to verify the performance of the proposed MFAC controller.

A. SIMULATION SCHEME

In this paper, the parafoil system is regarded as an SISO system, wherein the input is the asymmetric deflection of the steering lines and the output is the combination of the distance error and the heading angle error.

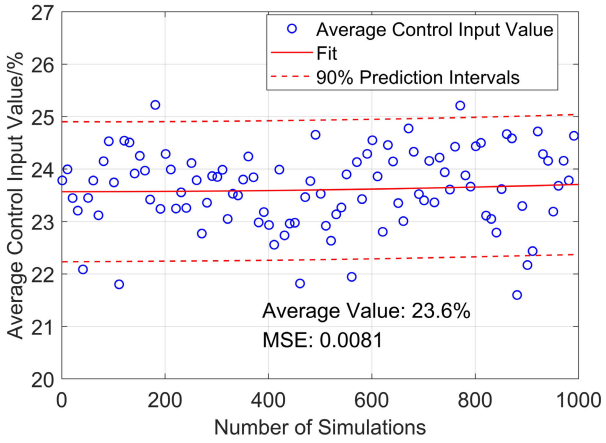

FIGURE 7. Distribution of the average control input value in 1000 simulations.

The framework of the simulation scheme is shown in Fig. 8. The real-time position and attitude data of the parafoil system are obtained by the dynamic model. The system error is composed of the distance error and the heading angle error integrated with the desired trajectory. In addition, considering the stall margin in the real control system, the maximum control deflection is limited to 80% [7]. The geometric parameters of the parafoil system in the simulation are listed in Table 2, and the aerodynamic coefficients are selected according to the data in Ref. [23].

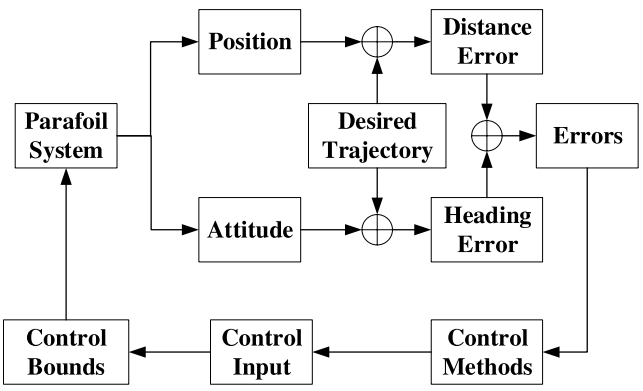

FIGURE 8. Simulation process.

TABLE 2. Geometric parameters of the parafoil system.

Parameters	Mass (kg)	b (m)	c (m)	S (m^2)
Values	2.4	1.35	0.75	1

B. SIMULATION CONDITIONS

During the simulation, three desired trajectories and three flight conditions are set. The three trajectories are a straight-line trajectory, a polyline trajectory composed of four straight line segments, and a circular trajectory with a straight-line segment. The three flight conditions are no disturbances,

gusty wind disturbances, and random disturbances, wherein the random disturbances include random disturbances in the wind field and random disturbances in the flight data, as shown in Table 1.

The control performance of the MFAC method is assessed and compared with that of the PID and ADRC methods. The designed controller parameters for each control method, which are shown in Table 3, remain the same during the following simulations.

TABLE 3. Control parameters for the different methods.

PID parameters	K_p	K_i	K_d	
Values	0.4	0	0.3	
ADRC parameters	W_0	W_c	b_0	
Values	0.2	1.2	1	
MFAC parameters	α	β	τ	κ
Values	0.01	1	0.1	0.1

VI. RESULTS

A. NO DISTURBANCES CONDITION

1) STRAIGHT-LINE TRAJECTORY

A straight-line trajectory is a basic and classical path to verify the performance of a controller. In this simulation, the expression of the segment is a positive linear function with a range of 0 m to 200 m. Fig. 9 indicates that the three controllers can control the parafoil system to accurately track the desired trajectory.

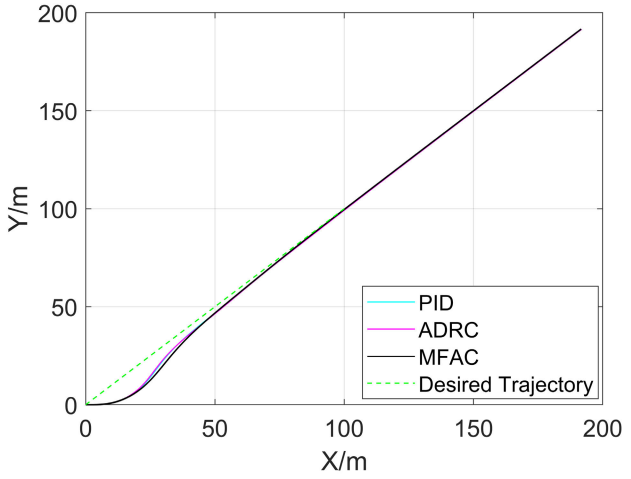

FIGURE 9. Straight-line trajectory control performance (no disturbances).

The corresponding distance error is shown in Fig. 10. All controllers can gradually control the distance error to approximately 0 m; the peak value of the distance error is approximately 10 m, which reduces to 1 m within 20 s. As shown in this figure, the MFAC controller has a slightly larger distance error and a higher convergence speed than the other controllers. In addition, the input process of the controllers is also analyzed, which reflects the control energy of the system to a certain extent, as shown in Fig. 11.

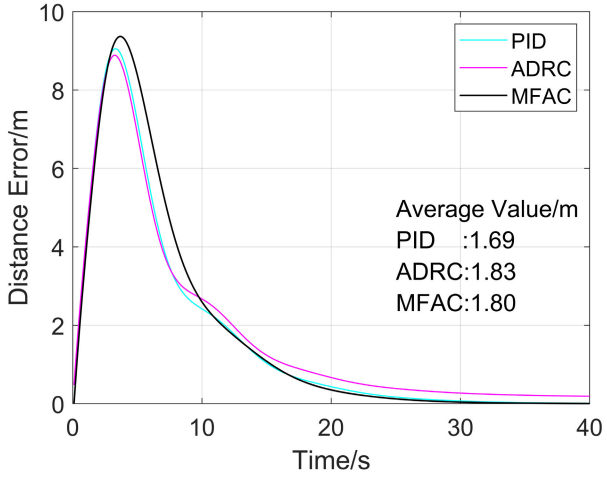

FIGURE 10. Distance error for the straight-line trajectory (no disturbances).

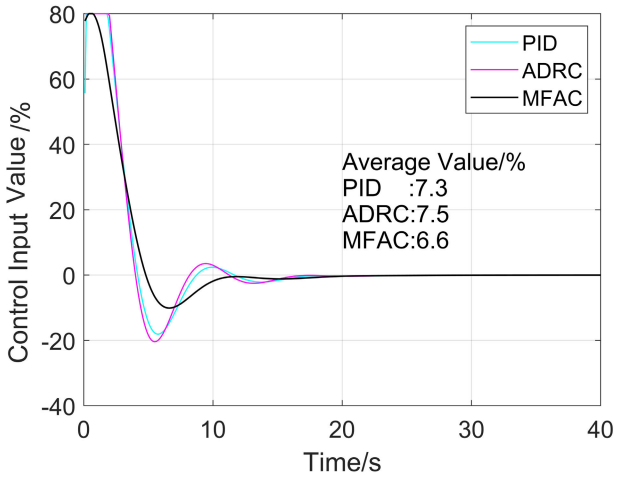

FIGURE 11. Control input value for the straight-line trajectory (no disturbances).

Fig. 11 shows that the value of the control input for the three controllers reaches 0% after 20 s and that the peak values of the control input occur at the same time as the peak values of the distance error. The maximum overshoot value of the control input and the average value of the MFAC controller are smaller than those of the other two controllers. The average input value of the MFAC controller is 91% of that of the PID controller and 89% of that of the ADRC controller, whereas the maximum overshoot value of the MFAC controller is only half of that of the other two controllers. Moreover, the standard deviations of the control input in this condition are 0.1896, 0.1935, and 0.1746 for the PID, ADRC, and MFAC controllers, respectively. Hence, the MFAC controller achieves the smallest standard deviation and the most stable control effect.

2) POLYLINE TRAJECTORY

In this section, a polyline trajectory composed of four straight lines is designed to verify the control performance in turning

points. Fig. 12 shows that the three controllers can control the parafoil system to accurately track the desired trajectory.

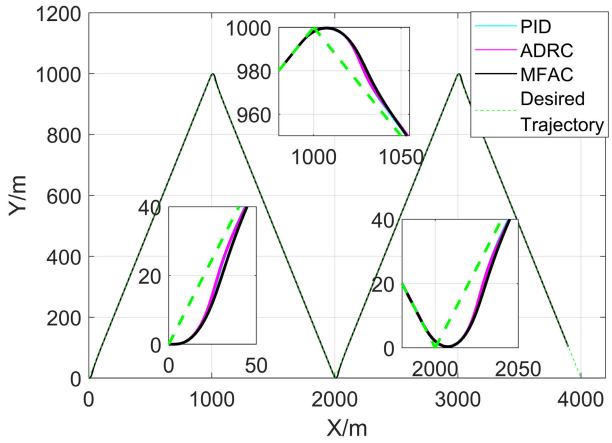

FIGURE 12. Control performance for the polyline trajectory (no disturbances).

As shown in Fig. 13, the peak values of the distance error occur at the three turning points and the starting point. A certain distance threshold (14.14 m in this case) is set to determine whether the parafoil has reached the turning point, which is the same time as the peak value of the distance error. The three controllers perform similarly in this condition with a similar average value of distance error.

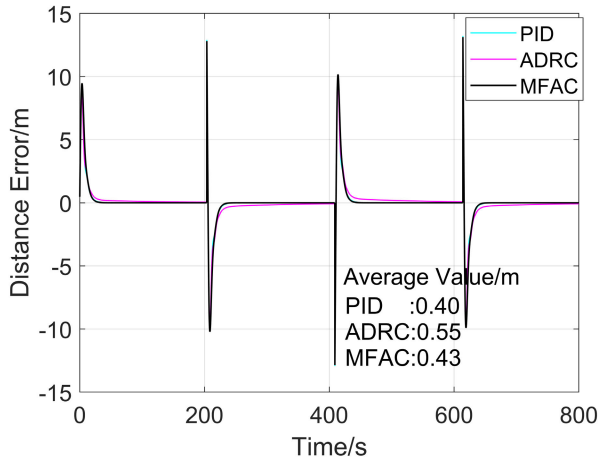

FIGURE 13. Distance error for the polyline trajectory (no disturbances).

Fig. 14 shows the control input value in this situation. The average value of the MFAC controller is less than that of the other two controllers. According to the established bounds, the control input reaches 80% at each turning point. The magnified parts in this figure show the value of the control input in detail at the second turning point. Obviously, the overshoot value of the MFAC controller is much smaller than those of the PID and ADRC controllers. From the entire control process, the average control input value of the MFAC controller is 90% of that of the PID controller and

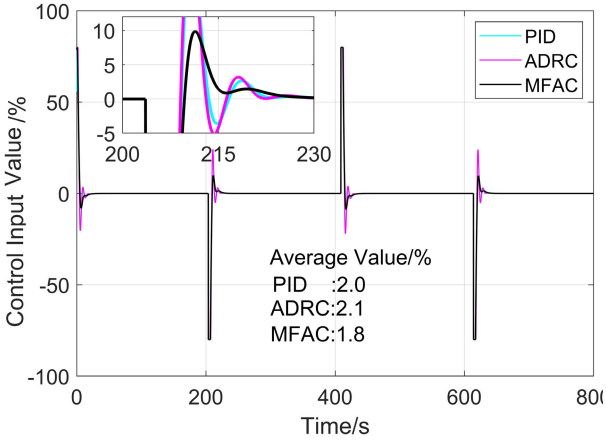

FIGURE 14. Control input value for the polyline trajectory (no disturbances).

86% of that of the ADRC controller. The standard deviations of the control input are 0.1106, 0.1118, and 0.1041 in the polyline trajectory situation for the PID, ADRC, and MFAC controllers, respectively.

3) CIRCULAR TRAJECTORY

A circular trajectory with a radius of 500 m is used to further verify the effectiveness of the MFAC controller. The initial position of the parafoil system is [-600 0] m. The entire circular trajectory is spit into 72 sections, wherein each section is treated as a segment during the simulation.

Fig. 15 shows that the three different controllers can make the parafoil system accurately track the circular trajectory. The magnified part in this figure is the turning point from the line segment to the circular path, where a substantial distance error occurs because the turning angle at this moment is the largest. In addition, as shown in Fig. 16, the distance error of the MFAC controller is smaller than those of the PID and ADRC controllers.

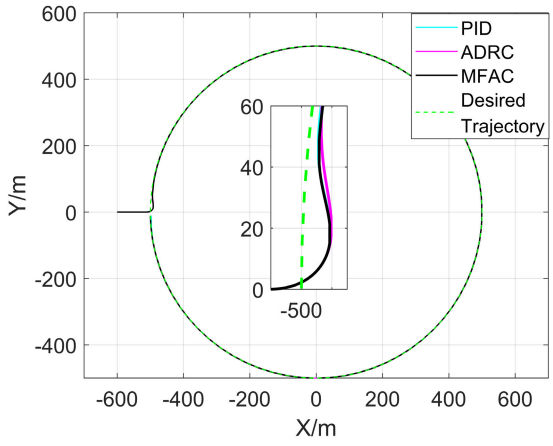

FIGURE 15. Control performance for the circular trajectory (no disturbances).

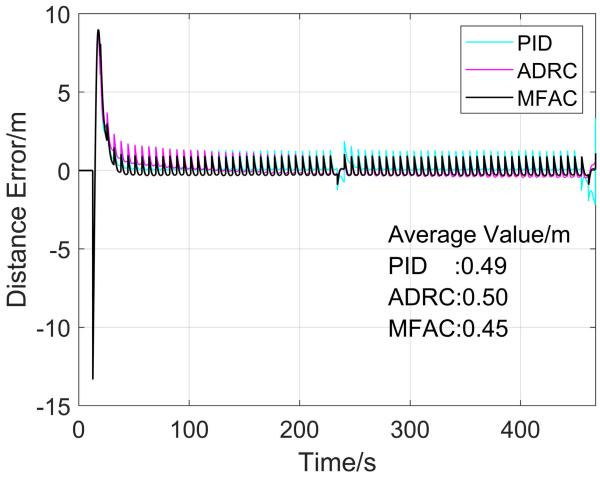

FIGURE 16. Distance error for the circular trajectory (no disturbances).

Similarly, the value of the control input of the MFAC controller is slightly less than that of the PID and ADRC controllers, as shown in Fig. 17. The MFAC controller achieves more stable control input with a standard deviation of 0.0749; in contrast, the standard deviation of the PID and ADRC controllers are 0.082 and 0.0821, respectively.

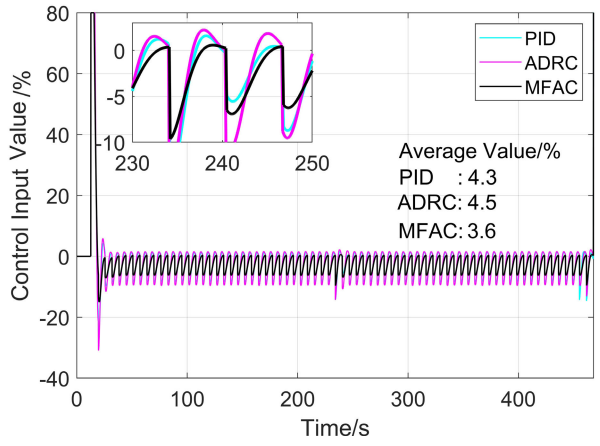

FIGURE 17. Control input value for the circular trajectory (no disturbances).

In the circular trajectory simulation, the MFAC controller performs better than the other controllers, as it has a smaller distance error, a lower average control input value, and a more stable control value.

According to the three simulations of various trajectories in the no disturbances condition, the performance of the MFAC controller is the best in most evaluation criteria, especially the average value and standard deviations of the control input.

B. GUSTY WIND DISTURBANCES CONDITION

Under this condition, simulations of gusty wind disturbances are carried out on three different trajectories to verify the robustness of the controllers. A gusty wind disturbance with a value of $[-4,0,0]^T$ m/s is added to the wind field once or twice during the simulations.

1) STRAIGHT-LINE TRAJECTORY

The control performance of the controllers in the straight-line trajectory is shown in Fig. 18, wherein the gusty wind disturbances are added to the wind field at 10–15 s. As shown in this figure, there is a sudden change during the tracking process, which is obviously different from the response in Fig. 9. Although the gusty wind changes twice, the three controllers drive the parafoil system to accurately match the polyline trajectory.

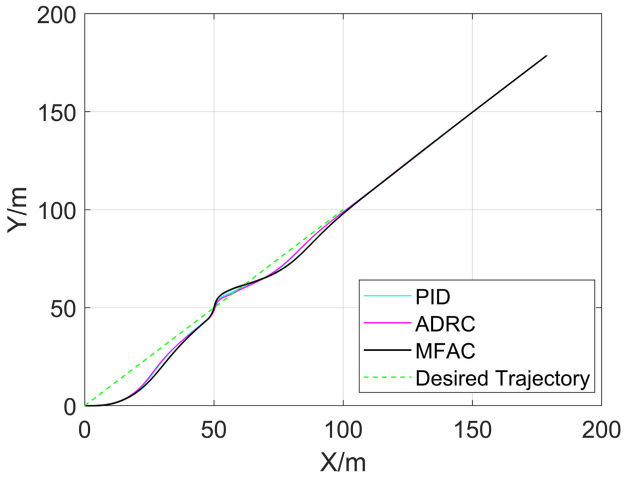

FIGURE 18. Control performance for the straight-line trajectory (gusty wind disturbances).

Fig. 19 shows the distance error in this trajectory, wherein the average value of the MFAC controller is slightly worse than that of the other controllers. As shown in Fig. 20, the average control input value of the MFAC controller is smaller than those of the PID and ADRC controllers. Additionally, the overshoot of the control input of the MFAC controller is much smaller than those of the other two controllers

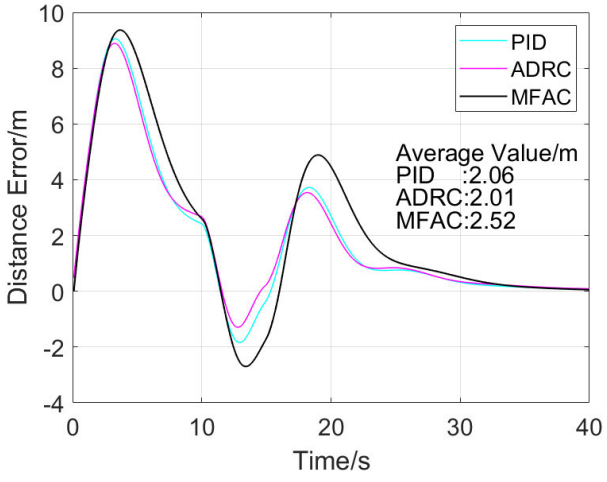

FIGURE 19. Distance error for the straight-line trajectory (gusty wind disturbances).

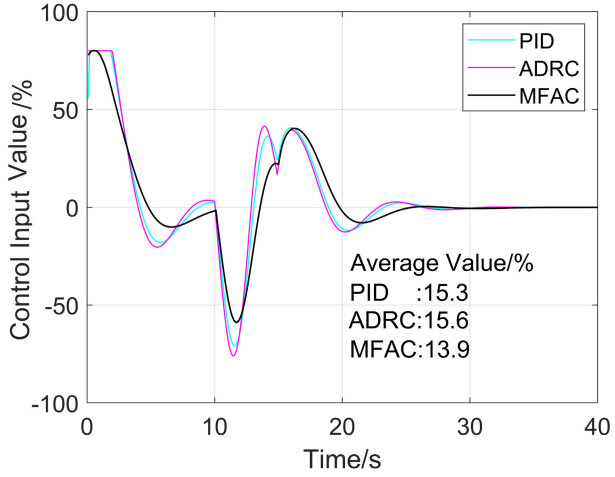

FIGURE 20. Control input value for the straight-line trajectory (gusty wind disturbances).

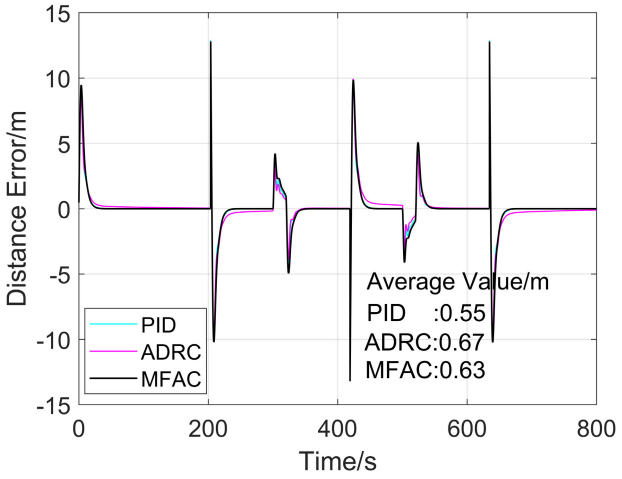

FIGURE 22. Distance error for the polyline trajectory (gusty wind disturbances).

at the point of the gusty wind disturbance. The standard deviations of the PID ADRC, and MFAC controllers are 0.2232, 0.2294, and 0.2038, respectively, which means that the MFAC controller is the most stable.

2) POLYLINE TRAJECTORY

In the polyline trajectory simulations, the gusty wind disturbances are added to the wind field at 300–320 s and 500–520 s. The control performance in this simulation is shown in Fig. 21, wherein the disturbance points are magnified. The control performance of the parafoil system at the turning points is the same as that under no disturbances. As shown in this figure, the three controllers can drive the system to accurately track the desired trajectory.

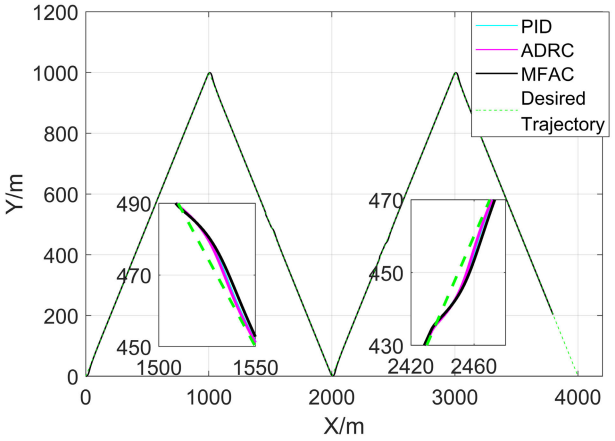

FIGURE 21. Control performance for the polyline trajectory (gusty wind disturbances).

Fig. 22 shows the distance error of the parafoil system from the desired trajectory. The ADEs of the three controllers are similar, and the most significant distance error is less than 5 m, which occurs at the gusty wind disturbance points.

Fig. 23 shows the value of the control input in the simulations, wherein the average value of the MFAC controller is 85% of that of the PID controller and 82% of that of the ADRC controller. The magnified part in this figure is the second disturbance point, which shows that the overshoot of the control input of the MFAC controller is much smaller and smoother than that of the other two controllers, which is the same as the results at the other disturbance point. The standard deviations of the control input are 0.1236, 0.1260, and 0.1128 for the PID, ADRC, and MFAC controllers, respectively.

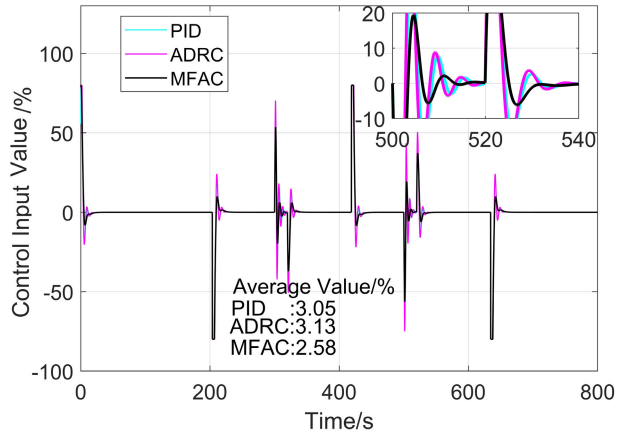

FIGURE 23. Control input value for the polyline trajectory (gusty wind disturbances).

3) CIRCULAR TRAJECTORY

Two gusty wind disturbances are added to the wind field at 100–120 s and 300–320 s in the circular trajectory simulations. As shown in Fig. 24, the control performance of the three controllers is good, even at the wind disturbance points. To clearly observe the performance at the disturbance points, two magnified parts are emphasized in this figure.

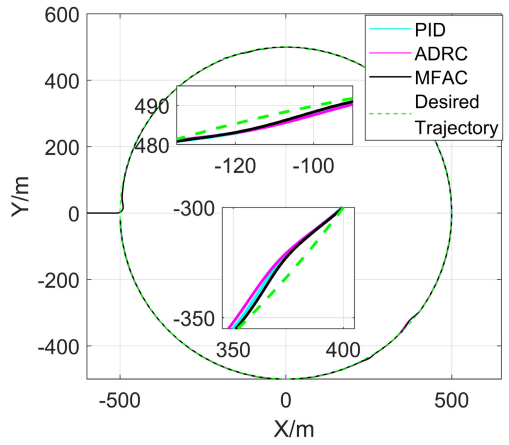

FIGURE 24. Control performance for the circular trajectory (gusty wind disturbances).

The distance error for the circular trajectory is shown in Fig. 25. During the entire simulation process, the ADE of the MFAC controller is less than 1 m, and the value is less than 2 m after the parafoil enters the circular path (except for the two disturbance points).

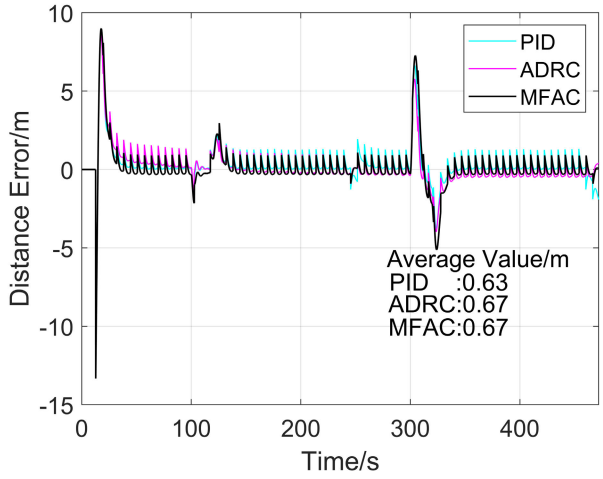

FIGURE 25. Distance error for the circular trajectory (gusty wind disturbances).

There are two points where the distance error substantially increases in this simulation, as shown in Fig. 25; these two points are the disturbance points, and the distance error at the second disturbance point is much larger than that at the first one. The gusty wind disturbance at the second point is in the same direction as the parafoil system heading, which results in a dramatic increase in the speed of the parafoil; the opposite scenario occurs at the first point. The ground speed of the parafoil system is shown in Fig. 26, wherein there is little difference in the results of the three different control methods.

The control input value in this simulation is shown in Fig. 27, which—similar to the distance error response plot—contained two notable changes. The average control

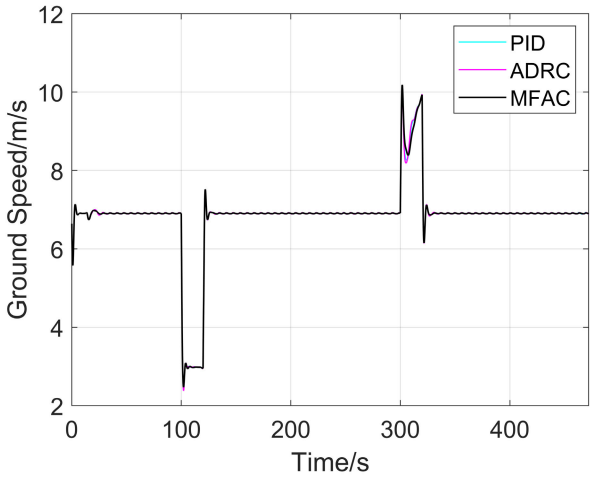

FIGURE 26. Ground speed (gusty wind disturbances).

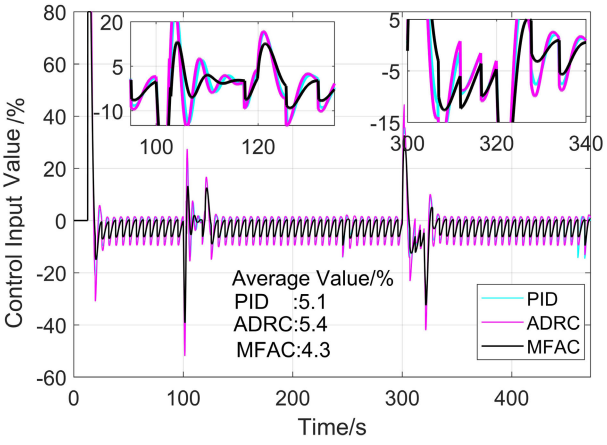

FIGURE 27. Control input value for the circular trajectory (gusty wind disturbances).

input value of the MFAC controller during this simulation is smaller than those of the PID and ADRC controllers. In addition, at the gusty wind points, the control input value of the MFAC controller is far less than those of the other two controllers, which means that the MFAC method has better robustness.

The standard deviations of the control input for the PID, ADRC, and MFAC controllers are 0.089, 0.0913, and 0.0808, respectively; hence, the MFAC controller is the most stable.

In the gusty wind situation, the three controllers can control the parafoil system to accurately track the desired trajectories. The MFAC method is superior to the other control methods in some indexes, especially the value of the control input, including the average value and the standard deviation.

C. RANDOM DISTURBANCES CONDITION

In a real flight environment, the wind field is not constant, and disturbances are mixed in the status data. To imitate a complicated real flight environment, disturbances are added to the wind field and parafoil system status data in the simulations.

The disturbances in the system status are listed in Table 1. The simulations show that the three controllers can drive the parafoil system along the desired trajectories, but the distance error and control input value are much larger than those in the other conditions.

In addition to the status data disturbances, the random wind is added to the constant wind field, wherein the constant wind is $[-4,0,0]^T$ m/s. The random wind fits a normal distribution, having a mean value of 0 m/s, and a standard deviation of 1. Hence, the random wind is different in every simulation, among which one of the possibilities is shown in Fig. 28.

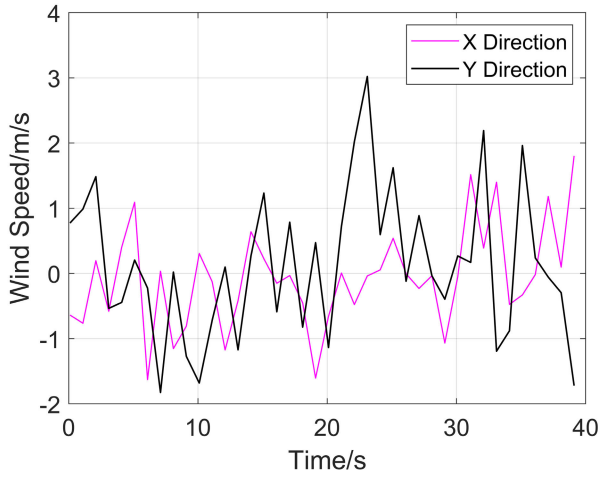

FIGURE 28. Random wind field.

1) STRAIGHT-LINE TRAJECTORY

As shown in Fig. 29, the three controllers drive the parafoil system to generally track the trajectory under the random disturbances situation. However, the control performance for the straight-line trajectory under these conditions is worse than that under the last two conditions. The distance error from the straight-line trajectory is shown in Fig. 30. This

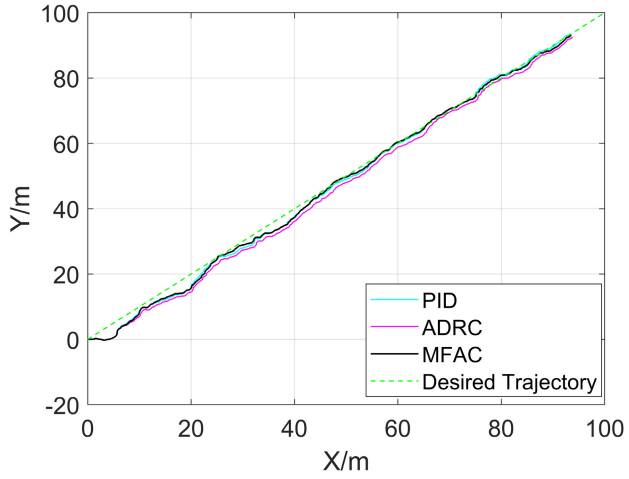

FIGURE 29. Control performance for the straight-line trajectory (random disturbances).

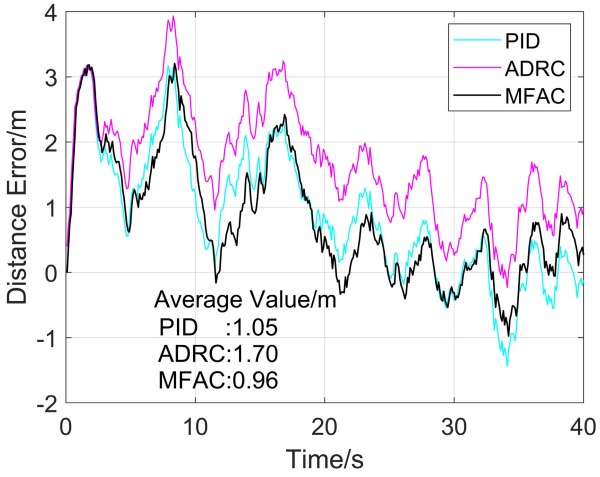

FIGURE 30. Distance error for the straight-line trajectory (random disturbances).

figure shows that the ADE of the MFAC controller is 0.96 m, which is the smallest value among all three controllers; note that this value is only 56.5% of that of the ADRC controller.

The control input value in this simulation is far greater than that in the simulations without disturbances, as shown in Fig. 31, wherein the points are shown at 0.5 s intervals. The average values of the control input for the PID, ADRC, and MFAC controllers are 35.0%, 43.7%, and 33.7%, respectively. Moreover, the standard deviations of the control input for these three controllers are 0.2469, 0.2693, and 0.2421, respectively. Hence, the MFAC controller achieves the smallest distance error with the least energy consumption in this simulation.

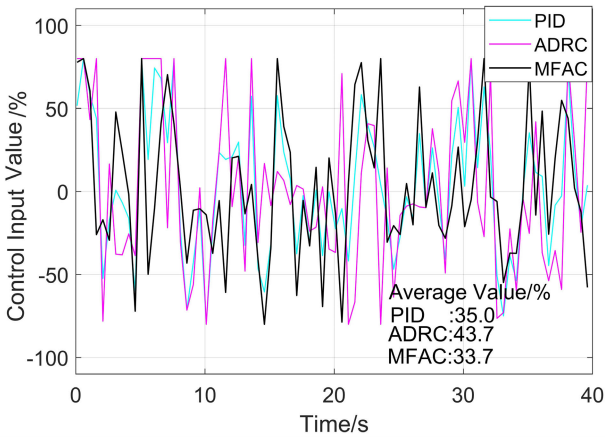

FIGURE 31. Control input value for the straight-line trajectory (random disturbances).

2) POLYLINE TRAJECTORY

The polyline trajectory is simulated in the random disturbances condition, for which the control performance is shown in Fig. 32. This figure shows that the three controllers drive the parafoil system to accurately track the polyline trajectory.

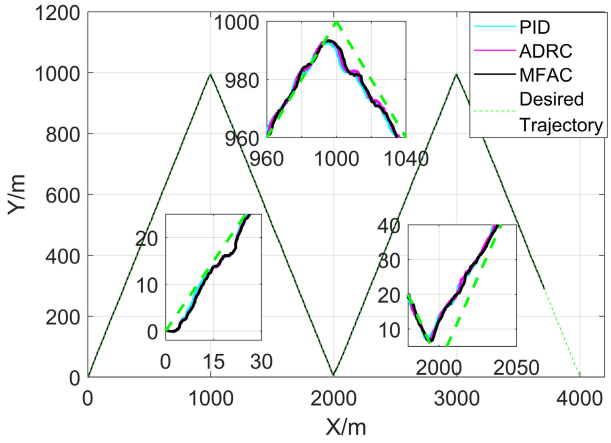

FIGURE 32. Control performance for the polyline trajectory (random disturbances).

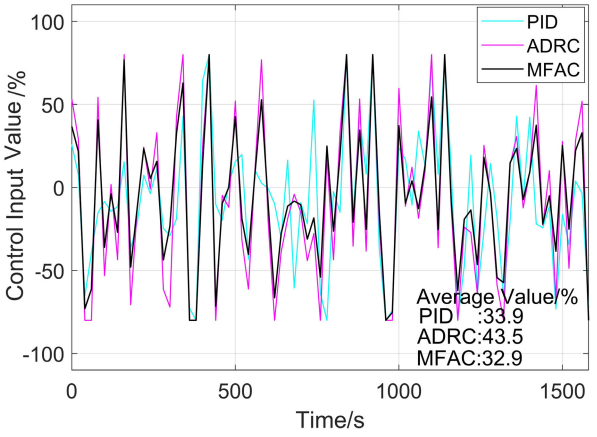

FIGURE 34. Control input value for the polyline trajectory (random disturbances).

Moreover, the turning points are magnified in this figure to show additional details.

Fig. 33 shows the distance error for the polyline trajectory, which more directly illustrates the control performance. The notable points in this plot are the turning points, which are approximately 14 m, which is the same as the threshold setting. The ADEs of each control method are less than 1 m, and the ADE of the MFAC controller is the smallest.

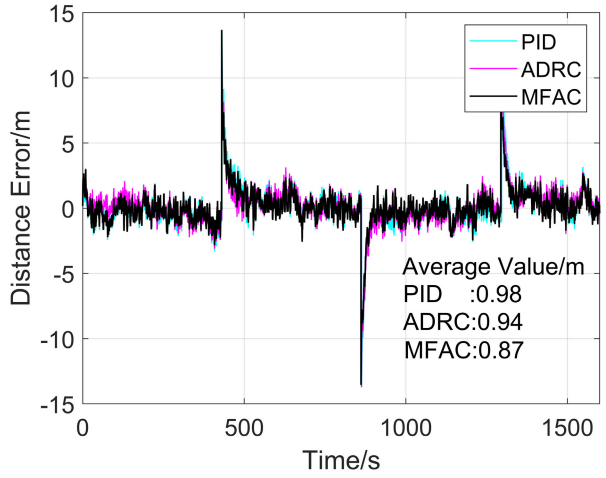

FIGURE 33. Distance error for the polyline trajectory (random disturbances).

The value of the control input is shown in Fig. 34, wherein the data are shown at 20 s intervals because the disturbances lead to sharp changes in the control input during the simulation. The average values of the control input for the MFAC, ADRC, and PID controllers are 32.9%, 43.5%, and 33.9%, respectively. Hence, the MFAC controller performs well compared with the other two methods and has the advantages of less energy consumption and higher precision. The standard deviations of these three controllers are 0.2393, 0.2703, and 0.2379, respectively. Thus, the PID control method and the MFAC method have similar stability.

3) CIRCULAR TRAJECTORY

The circular trajectory is simulated in the random disturbances condition, for which the control performance is shown in Fig. 35. This figure shows that the parafoil system accurately follows the trajectory under the three controllers in this simulation, wherein the maximum error occurs at the entry point from the line segment to the circle.

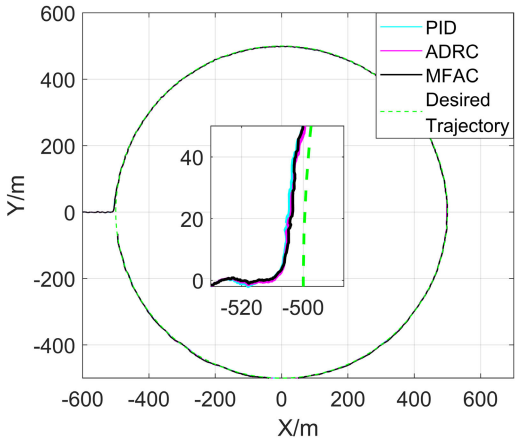

FIGURE 35. Control performance for the circular trajectory (random disturbances).

Fig. 36 shows the distance error from the trajectory, wherein the ADEs for the PID, ADRC, and MFAC controllers are 1.19 m, 1.25 m, and 1.14 m, respectively. Hence, the PID and the MFAC controller have similar values.

The value of the control input in this simulation is shown in Fig. 37. The average values of the control input for the PID, ADRC, and MFAC controllers are 30.0%, 39.5%, and 29.6%, respectively. Moreover, the standard deviations of these three controllers are 0.2356, 0.2676, and 0.2337, respectively.

In the circular trajectory simulation, the MFAC controller achieves a higher precision and a smaller and more stable control input than the other two controllers.

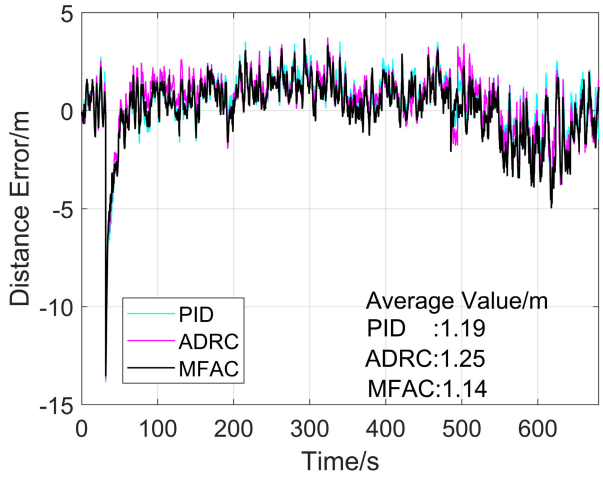

FIGURE 36. Distance error for the circular trajectory (random disturbances).

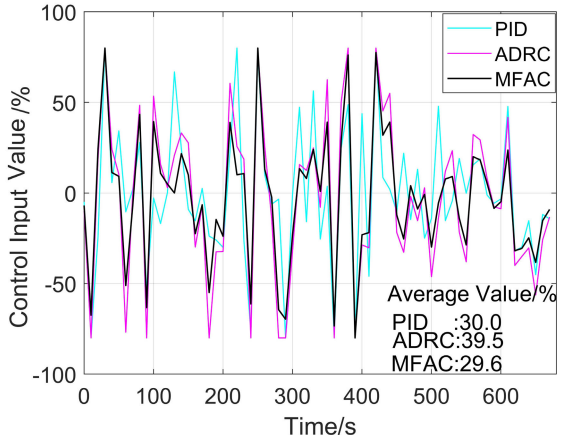

FIGURE 37. Control input value for the circular trajectory (random disturbances).

In this section, a random wind field and status data disturbances are added to the simulations to imitate real flight conditions, and the results showed that the three controllers can generally drive the parafoil system to accurately track the desired trajectories. The MFAC controller performs better than the other controllers with less energy consumption and higher precision.

VII. CONCLUSION

This paper introduces a novel real-time model-independent trajectory control method for parafoil systems, which is called the MFAC method. The stability of the MFAC method is theoretically verified, and the robustness of this approach is analyzed and demonstrated by the Monte Carlo method. To further evaluate the control performance, a six-DOF model of the parafoil system is built, and a series of simulation tests are performed under various conditions: no disturbances, gusty wind disturbances, and random disturbances. This proposed method can eliminate the influences of inaccurate models and external disturbances and enables the parafoil system to track desired trajectories.

The simulation results for the MFAC controller are compared with those of the PID and ADRC controllers commonly used in parafoil systems. These comparisons demonstrated that the MFAC controller is as effective as the PID and ADRC controllers. All three control controllers can make the parafoil system accurately track the desired paths. Additionally, the ADE and the standard deviation of the control input value for the MFAC controller are mostly smaller than those for the PID and ADRC controllers, especially under disturbance conditions. The MFAC controller also has the smallest overshoot of the control input value among the three controllers. Hence, the proposed control method has advantages in terms of control precision and energy consumption.

In this paper, a theoretical proof and numerical simulation of the MFAC controller for parafoil systems are presented. The following study will apply the MFAC method to an actual parafoil system and verify the control performance of this method through flight tests.

REFERENCES

[1] J. Tao, M. Piao, Q. Sun, M. Sun, and Z. Chen, "Tracking control of parafoil airdrop robot in wind environments," in *Proc. 11th Int. Workshop Robot Motion Control (RoMoCo)*, Wasowo, Poland, Jul. 2017, pp. 269–274.

[2] W. Wailes, "Advanced recovery systems for advanced launch vehicles (ARS) phase 1study results," in *Proc. 10th Aerodynamic Decelerator Conf.*, Cocoa Beach, FL, USA, Apr. 1989, p. 881.

[3] F. Lv, W. He, and L. Zhao, "An improved nonlinear multibody dynamic model for a parafoil-UAV system," *IEEE Access*, vol. 7, pp. 139994–140009, 2019.

[4] E. Mooij, Q. Wijnands, and B. Schat, "9 DOF parafoil/payload simulator development and validation," in *Proc. AIAA Modeling Simulation Technol. Conf. Exhibit*, Austin, TX, USA, Aug. 2003, pp. 11–14.

[5] N. Slegers and M. Costello, "Aspects of control for a parafoil and payload system," *J. Guid., Control, Dyn.*, vol. 26, no. 6, pp. 898–905, Nov. 2003.

[6] O. A. Yakimenko, *Precision Aerial Delivery Systems: Modeling, Dynamics, and Control*. Reston, VA, USA: AIAA, 2015, pp. 281–287.

[7] T. Bennett and R. Fox, "Design, development & flight testing of the NASA X-38 7500 ft2 parafoil recovery system," in *Proc. 17th AIAA Aerodyn. Decelerator Syst. Technol. Conf. Seminar*, Monterey, CA, USA, 2003, pp. 1–7.

[8] J. W. Wegereef and H. Jentink, "SPADES: A parafoil delivery system for payloads until 200 kg," in *Proc. 17th AIAA Aerodynamic Decelerator Syst. Technol. Conf. Seminar*, Monterey, CA, USA, May 2003, p. 2110.

[9] N. Slegers and M. Costello, "Model predictive control of a parafoil and payload system," *J. Guid., Control, Dyn.*, vol. 28, no. 4, pp. 816–821, Jul. 2005.

[10] J. Tao, Q. Sun, H. Sun, Z. Chen, M. Dehmer, and M. Sun, "Dynamic modeling and trajectory tracking control of parafoil system in wind environments," *IEEE/ASME Trans. Mechatronics*, vol. 22, no. 6, pp. 2736–2745, Dec. 2017.

[11] D. Carter, S. George, P. Hattis, M. W. McConley, S. Rasmussen, L. Singh, and S. Tavan, "Autonomous large parafoil guidance, navigation, and control system design status," in *Proc. 19th AIAA Aerodynamic Decelerator Syst. Technol. Conf. Seminar*, May 2007, pp. 1–7.

[12] S. Liu, Z. Hou, Y. Guo, and L. Guo, "A novel modified robust model-free adaptive control method for a class of nonlinear systems with time delay," in *Proc. IEEE 8th Data Driven Control Learn. Syst. Conf. (DDCLS)*, Dali, China, May 2019, pp. 1329–1334.

[13] Y. Guo, Z. Hou, S. Liu, and S. Jin, "Data-driven model-free adaptive predictive control for a class of MIMO nonlinear discrete-time systems with stability analysis," *IEEE Access*, vol. 7, pp. 102852–102866, 2019.

[14] R. Cao, Z. Hou, Y. Zhao, and B. Zhang, "Model free adaptive iterative learning control for tool feed system in noncircular turning," *IEEE Access*, vol. 7, pp. 113712–113725, 2019.

[15] B. Gao, R. Cao, Z. Hou, and H. Zhou, "Model-free adaptive MIMO control algorithm application in polishing robot," in *Proc. 6th Data Driven Control Learn. Syst. (DDCLS)*, Chongqing, China, May 2017, pp. 135–140.
[16] R. Zhang and Z. Hou, "Iterative learning control for nonlinear MIMO systems with unknown nonparametric uncertainties and input saturations," in *Proc. 27th Chin. Control Decision Conf. (CCDC)*, Qingdao, China, May 2015, pp. 1085–1089.
[17] J. Liu, X. Yu, S. Jin, and Z. Hou, "Model free adaptive attitude control for a launch vehicle," in *Proc. Chin. Control Conf. (CCC)*, Guangzhou, China, Jul. 2019, pp. 8218–8223.
[18] Z. Yang, X. Yu, S. Jin, and Z. Hou, "Model free adaptive attitude control of launch vehicle using iterative feedback tuning," in *Proc. IEEE 8th Data Driven Control Learn. Syst. Conf. (DDCLS)*, Dali, China, May 2019, pp. 1196–1201.
[19] Q. Jiang, Y. Liao, Y. Li, J. Fan, and Y. Miao, "Heading control of unmanned surface vehicle with variable output constraint model-free adaptive control algorithm," *IEEE Access*, vol. 7, pp. 131008–131018, 2019.
[20] O. A. Yakimenko, *Precision Aerial Delivery Systems: Modeling, Dynamics, and Control*. Reston, VA, USA: AIAA, 2015, pp. 264–269.
[21] Z. Hou and Y. Zhu, "Model based control and mfac, which is better in simulation?" in *Proc. IFAC*, Shanghai, China, 2013, pp. 82–87.
[22] Z. Hou, "MFAC for MISO discrete-time nonlinear system," in *Model Free Adaptation Control: Theory Applications*, 1st ed. Beijing, China: Science Press, 2013, pp. 92–100.
[23] O. A. Yakimenko, *Precision Aerial Delivery Systems: Modeling, Dynamics, and Control*. Reston, VA, USA: AIAA, 2015, p. 289.
[24] N. Slegers, E. Beyer, and M. Costello, "Use of variable incidence angle for glide slope control of autonomous parafoils," *J. Guid., Control, Dyn.*, vol. 31, no. 3, pp. 585–596, May 2008.

LINGGONG ZHAO received the B.S. degree in applied physics from Shandong University, Jinan, China, in 2011, and the M.S. degree in spacecraft engineering from Beihang University, Beijing, in 2014. He is currently pursuing the Ph.D. degree in aeronautical and astronautical science and technology with the School of Astronautics, Beihang University.

His research interests include parafoil systems design and unmanned aerial vehicle control.

WEILIANG HE received the B.S. degree in aircraft design from the Nanjing University of Aeronautics and Astronautics, Nanjing, China, in 1987, the M.S. degree in spacecraft engineering from the China Academy of Space Technology, Beijing, China, in 1990, and the Ph.D. degree in spacecraft engineering from Beihang University, Beijing, in 2006.

His research interests include spacecraft system design, spacecraft reentry, landing technology, and inflatable space structure systems.

FEIKAI LV received the B.S. degree in aircraft design and engineering from Northwestern Polytechnical University, Xi'an, in 2010, and the M.S. degree in spacecraft engineering from Beihang University, Beijing, in 2014, where he is currently pursuing the Ph.D. degree in spacecraft engineering with the School of Astronautics.

His research interests include modeling and simulation, flight dynamic, and robust control for parafoil systems.

WANG XIAOGUANG was born in Pingdingshan, China. He received the M.S. degree in spacecraft engineering from Beihang University, Beijing, in 2015, where he is currently pursuing the Ph.D. degree in spacecraft engineering with the School of Astronautics.

His research interests include modeling updating, parameter identification, and uncertainty quantification and analysis.